



## Photocrosslinking Polymeric Ionic Liquids via Anthracene Cycloaddition for Organic Electronics

Journal:	<i>Journal of Materials Chemistry C</i>
Manuscript ID	TC-ART-05-2018-002561.R1
Article Type:	Paper
Date Submitted by the Author:	16-Jul-2018
Complete List of Authors:	<p>Popere, Bhooshan; UC Santa Barbara,  Sanoja, Gabriel; University of California-Santa Barbara, Dept. of Chemical Engineering  Thomas, Elayne; University of California, Santa Barbara, Materials Department  Schauer, Nicole; University of California, Materials Department  Jones, Seamus; University of California-Santa Barbara, Dept. of Chemical Engineering  Bartels, Joshua; University of California-Santa Barbara, Dept. of Chemical Engineering  Helgeson, Matthew; UC Santa Barbara, Chemical Engineering  Chabinyk, Michael; University of California, Materials Department  Segalman, Rachel; University of California-Santa Barbara, Dept. of Chemical Engineering</p>

# Photocrosslinking Polymeric Ionic Liquids *via* Anthracene Cycloaddition for Organic Electronics

*Bhooshan C. Popere,<sup>1,†,§</sup> Gabriel E. Sanoja,<sup>1,3,†,‡</sup> Elayne M. Thomas,<sup>2</sup> Nicole S. Schausser,<sup>2</sup> Seamus D. Jones,<sup>1</sup> Joshua M. Bartels,<sup>1</sup> Matthew E. Helgeson,<sup>1</sup> Michael L. Chabinyc,<sup>2</sup> and Rachel A. Segalman<sup>1,2\*</sup>*

<sup>1</sup>Department of Chemical Engineering and <sup>2</sup>Materials Department, University of California, Santa Barbara, California, 93106, United States

<sup>3</sup>Department of Chemical and Biomolecular Engineering, University of California, Berkeley, California, 94720, United States

\*Email address: [segalman@ucsb.edu](mailto:segalman@ucsb.edu)

<sup>†</sup>Equal contribution

**Abstract**

Polymeric ionic liquids (*i.e.*, PILs) are single ion-conducting materials that exhibit the thermal and electrochemical stability of ionic liquids and the mechanical properties of polymers. Although PILs are exciting for a variety of applications in energy conversion and storage, the tradeoff between mechanics and ion transport remains an important limitation in materials design. Herein, a photocrosslinkable PIL based on the cycloaddition reaction of anthracene is converted from a viscous liquid into a soft solid without detrimental effects on the bulk ionic conductivity. The independent control of mechanical- and ion-conducting properties results from negligible changes in polymer segmental dynamics (*i.e.*, glass transition temperature) upon crosslinking. This was demonstrated for both a polymer (*i.e.*,  $N = 279$ ) and its corresponding oligomer (*i.e.*,  $N = 10$ ). The ease of processability facilitated by the presented molecular design is illustrated by both patterning the PIL into  $\mu\text{m}$ -sized features, and incorporating it as a dielectric in thin-film transistors for low-voltage operation independent of device fabrication geometry.

## Introduction

Polymeric ionic liquids (PILs) are an emerging class of functional materials that synergistically combine the ionic conductivity and thermo-electrochemical stability of ionic liquids (ILs) with the mechanical robustness of polymer scaffolds.<sup>1-3</sup> In contrast with ILs and polymer/IL blends where both the cation and the anion are mobile,<sup>4-6</sup> single-ion conducting PILs have one ion tethered to the polymer backbone.<sup>2</sup> Ionic conduction being an inherent material property, most PILs have been studied within the context of solid-state electrolytes or ion-conducting membranes for electrochemical systems,<sup>7</sup> and of particular interest herein dielectrics for organic electronic devices.<sup>8-11</sup> However, their unique set of physicochemical properties endowed by the chemical structure of the component ions makes them highly desirable for other applications including heavy metal ion adsorption,<sup>12</sup> gas capture and separations,<sup>13</sup> catalysis,<sup>14</sup> among others.<sup>3</sup>

PILs are promising dielectrics for organic electronics because they allow fine control over semiconductor charge carrier concentration *via* electrochemical doping. Similar to polymer/IL blends (*i.e.*, ion gels)<sup>15-17</sup> the high capacitance of their electrical double layer (1–10  $\mu\text{F}\cdot\text{cm}^{-2}$ ) induces large sheet carrier densities, which are not accessible with conventional gate insulators (*e.g.*,  $\text{SiO}_2$ ), while enabling low-voltage operation.<sup>8-11</sup> Polyelectrolyte gate insulators, where a proton typically acts as the cation, have also been proven to effectively induce large sheet carrier densities in thin-film transistors.<sup>18, 19</sup> Interestingly, the single-ion conducting (*i.e.*, unipolar) nature of PILs is suitable for fabrication of complementary *p*- and *n*-type devices necessary to develop integrated circuits, as either cations or anions can in principle be tethered to the polymer backbone. Given that the performance of dielectrics is strongly related to their ionic

conductivity and mechanical integrity, the range of PILs explored for organic electronics is similar to that investigated for solid-state electrolytes or ion-conducting membranes in electrochemical devices (*e.g.*, block copolymers).<sup>9</sup> However, there are important requirements in terms of dielectric processing that are still necessary for industrial scale manufacturing of integrated circuits. In particular, the ability to pattern these materials with photolithography would facilitate high-throughput, high-definition, and low-cost fabrication. Though patterning of polymer/IL blends has been demonstrated through a transfer printing method<sup>20</sup> and aerosol jet printing,<sup>16</sup> direct patterning of ion-conducting dielectrics remains elusive, both because the polymer scaffolds (*e.g.*, PS-*b*-PEO-*b*-PS and PVDF) are incompatible with photolithography, and because IL leaching limits spatial resolution. Thus, it is critical to design solution- and melt-processable PILs with decoupled mechanical and ion conducting properties.

PILs exhibit a significantly lower ionic conductivity than ILs and polymer/IL blends due to the low ion mobility intrinsic to viscous polymers and immobilization of 50 % of the ions.<sup>2</sup> Detailed investigations of PILs with varying architectures illustrate a strong dependence of ionic conductivity and mechanics not only on the polymer backbone, but also on the chemistry of the ions and their placement relative to the main chain.<sup>21, 22</sup> Molecular design strategies to enhance room-temperature anhydrous ionic conductivities in PILs include incorporation of plasticizers that efficiently solvate ions,<sup>23</sup> long and flexible linkers that position the IL moieties further away from the polymer chain,<sup>24</sup> and backbones with inherently low  $T_g$ .<sup>25</sup> The resulting PILs are high-viscosity and low-modulus polymers revealing a somewhat orthogonal relationship between ion conduction and mechanical robustness.

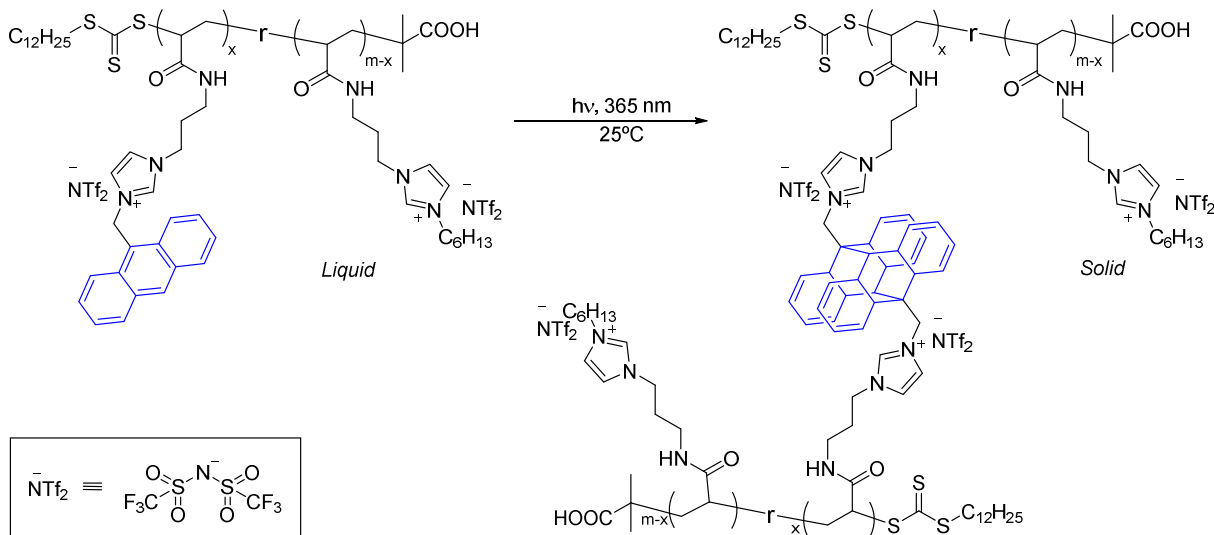
A promising strategy to decouple mechanical- and ion-conducting properties is to utilize block copolymers, wherein one of the blocks is composed of a glassy insulator and the other of a

low- $T_g$  ion conductor.<sup>26,27</sup> Studies on block copolymers based on PILs have provided invaluable insights into the role of structure on ionic conductivity,<sup>28-35</sup> yet the bulk performance of such materials is critically dependent on the long-range ion transport enabled by the alignment and connectivity of the conducting domains. An alternative strategy is based on ion-conducting polymer networks generated from copolymerization of IL monomers with varying content of multi-functional crosslinkers.<sup>36</sup> The properties of these materials are often challenging to optimize, as they are sensitive to the chemical composition during synthesis.<sup>37</sup> More importantly, ion-conducting polymer networks generally exhibit drastic reductions in the ionic conductivity upon crosslinking due to detrimental effects on segmental dynamics and ion mobility.

The incorporation of dynamic moieties based on a specific bond that breaks and reforms upon exposure to an external stimulus (*e.g.*, light, heat, stress, and chemical) constitutes a well-explored molecular design for stiffening<sup>38</sup> and patterning<sup>39</sup> polymers. However, the concomitant effects of such a strategy on bulk functional properties such as the ionic conductivity, particularly when these dynamic moieties are ionic in nature, remain unexplored. Herein, we report a photo-responsive PIL that can be readily converted from a high viscosity liquid into a flexible, and soft solid *via* the  $[4\pi + 4\pi]$  cycloaddition reaction of anthracene (Scheme 1). Upon exposure to 365 nm UV radiation, the PIL mechanical properties can be enhanced due to a topological change from an associated polymer to a lightly crosslinked chemical network. Interestingly, the PIL ionic conductivity remains unaffected due to the negligible differences in ion concentration, polymer segmental dynamics, and ion mobility upon crosslinking. Consequently, the presented molecular design demonstrates photo-induced formation of single-ion conducting PILs wherein the mechanical properties are tuned entirely independently of ion conduction. The material processability enabled by this strategy is useful for applications such as

patterning substrates with  $\mu\text{m}$ -size features, gating semiconductors in a thin-film geometry, among others.

**Scheme 1. Dimerization of anthracene enables conversion of a PIL from a polymer liquid to a soft solid.** This is enabled by conservation of molecular orbital symmetry in the photochemical  $[4\pi + 4\pi]$  cycloaddition of anthracene in the absence of  $\text{O}_2$ , a competing  $[4\pi + 2\pi]$  dienophile.



## Results and Discussion

Ion transport in polymers is anticipated to be intimately coupled to ion-polymer associations (*i.e.*, solvation) and polymer segmental dynamics. The former results from the succession of dissociative steps that facilitate ion hopping between neighboring solvating sites, whereas the latter from the excluded volume interactions that require polymer segments to accommodate space upon ion motion.<sup>40</sup> While solvation is important in conventional polymer electrolytes (*e.g.*, PEO/LiNTf<sub>2</sub>) where cations that form labile bonds with the backbone can have a significant contribution to the ionic conductivity, it is less so in single-ion conducting PILs due to the weak electrostatic interactions intrinsic to ionic liquid moieties.<sup>6</sup> Consequently, the ionic conductivity of PILs primarily depends on local dynamics as in concentrated liquid electrolytes<sup>41</sup> or multicomponent inert gases.<sup>42</sup> This molecular-level interconnection between ion motion and

polymer segmental dynamics is at the core of the long-standing tradeoff between bulk mechanics and ion transport in polymeric materials.

To circumvent this performance limitation, a PIL was designed that, upon exposure to an external stimulus, undergoes changes in mechanical properties without detrimental effects on the polymer segmental dynamics (*i.e.*,  $T_g$ ) and ion mobility. *A priori*, this is challenging because the degree of crosslinking generally influences the local configurational arrangement of polymer chains, and hence, the energy required for an ion to overcome the excluded volume interactions.<sup>43</sup> The proposed molecular design is based on dynamic polymer networks composed of stimuli-responsive, ionic, and transient junctions with weak binding energies (*i.e.*,  $\approx k_B T$ ) and association lifetimes that provide the material with longer terminal relaxation times and higher plateau moduli relative to polymer melts.<sup>44-47</sup> Upon activation with an external stimulus, these transient junctions are converted into their permanent counterparts to change the terminal mechanical response from that of a polymer liquid to that of a lightly crosslinked polymer network while (i) mitigating changes in  $T_g$  and ion mobility, (ii) decoupling mechanical- and ion-conductive properties, and (iii) enabling the simple processing necessary to incorporate PILs in a realm of organic electronic devices.

From a synthetic standpoint, we incorporated anthracene ionic groups in a PIL that dynamically associate via  $\pi$ - $\pi$  interactions. Irradiation with UV light (365 nm) triggers the photodimerization of these moieties via a  $[4\pi + 4\pi]$  cycloaddition reaction due to conservation of molecular orbital symmetry in the first-excited electronic state<sup>48, 49</sup> without inducing changes in the ion concentration. As described in the Supporting Information, an imidazole-functionalized precursor was synthesized *via* controlled-radical RAFT polymerization of N-acryloxysuccinimide (NASI), followed by nucleophilic substitution of an activated ester with 1-

(3-aminopropyl)imidazole. This polymer was exhaustively quaternized with mixtures of 9-chloromethylantracene and 1-bromohexane to yield a stable alkyl-substituted N-vinylimidazolium halide.<sup>50</sup> The halide-containing polymer was subsequently anion exchanged with a 10-fold molar excess of lithium bis(trifluoromethylsulfonyl)imide (LiNTf<sub>2</sub>) to afford a photocrosslinkable PIL with weak electrostatic interactions resulting from large, charge-delocalized, and ‘plasticizing’ ions that provide the material with a sub-ambient  $T_g$  even at high ion concentrations. The properties of these well-defined and narrowly-dispersed polymers, as determined with Gel Permeation Chromatography (GPC), <sup>1</sup>H Nuclear Magnetic Resonance (NMR), and Differential Scanning Calorimetry (DSC) are summarized in Table 1. We report the dispersity ( $\mathcal{D}$ ) of the precursor PNASI (Figure S1) because the electrostatic interactions between the PIL charged groups and the chromatography column result in unreliable characterization via GPC,<sup>51</sup> and the molecular weight distribution is not expected to be sensitive to the post-modification reactions. We incorporated sufficient anthracene moieties to afford photocrosslinking while still enabling a  $T_g$  below room temperature. Moreover, we note that the polymer segmental dynamics are likely dominated by ion concentration as opposed to molecular weight since the 10PIL exhibits a higher  $T_g$  than the 300PIL (Figure S5). The dependence of  $T_g$  on ion concentration is ubiquitous in ion-containing polymers (*e.g.*, ionomers,<sup>52</sup> polymer-salt mixtures,<sup>53</sup> polymer-ionic liquid blends,<sup>54</sup> or polymeric ionic liquids<sup>30</sup>) though the physical phenomena that dictates the direction of the shift upon incorporation of charges is still under investigation.

**Table 1.** Properties of photocrosslinkable PILs. <sup>a</sup>Polymers are labeled NPIL, where  $N$  is the degree of polymerization. <sup>b</sup>Determined *via* <sup>1</sup>H NMR end-group analysis (Figure S2); <sup>c</sup>Determined against narrow polystyrene standards by GPC (Figure S1). <sup>d</sup>Determined by differential scanning calorimetry (DSC) using the half-height step in heat capacity of the second heating curve (Figure S5).

Polymer <sup>a</sup>	$D_p^b$	$\mathcal{D}^c$	Anthracene mol% <sup>b</sup>	$T_g^d$ (liquid)	$T_g^d$ (solid)
----------------------	---------	-----------------	------------------------------	------------------	-----------------

---

10PIL	10	1.2	22	19°C	19°C
300PIL	279	1.2	8	-7°C	-7°C

---

The anthracene moieties ( $\lambda_{\text{max}} \approx 370$  nm) in the PIL undergo a  $[4\pi + 4\pi]$  cycloaddition reaction upon exposure to UV radiation, as demonstrated by the evolution of the absorbance spectra for 10PIL (inset of Figure 1a).<sup>55-59</sup> Upon irradiation in an inert environment, the absorption arising from the anthracene optical transitions progressively decreases due to a consumption of anthracene with a concomitant increase in the photodimerization product dianthracene. Note that only in the absence of oxygen, a competing dienophile that can undergo a  $[4\pi + 2\pi]$  Diels-Alder reaction with anthracene, the photodimer dianthracene is the major cycloaddition product and the PIL topologically changes from an associated polymer to a lightly crosslinked chemical network. Although it is difficult to obtain direct evidence of the cycloaddition product, byproduct, and reaction intermediates,<sup>60</sup> some insights into the reaction mechanism can be provided by a kinetic model (Supporting Information) describing the photochemical excitation and radiative decay of anthracene, intersystem crossing, and formation of dianthracene. The resulting rate law is consistent with the observed change in absorbance over time (Figure 1a) and yields a dimerization rate constant of  $1.3 \times 10^{-3} \text{ s}^{-1}$ , a value significantly lower than that of anthracene photodimerization in solution<sup>61</sup> and consistent with the higher reaction activation energy expected in a viscous polymer. Consequently, anthracene photodimerization potentially enables fine control over the PIL mesoscopic structure and bulk physicochemical properties.

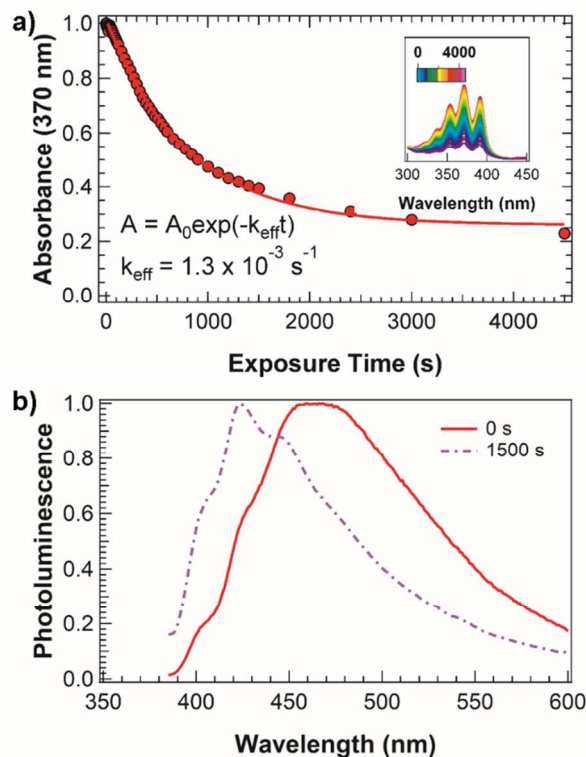


**Figure 1.** a) Normalized absorbance of the anthracene peak at 370 nm (●) progressively decreases with exposure time. The film thickness was  $\sim 1.5 \mu\text{m}$  and the irradiation wavelength 365 nm. The time constant obtained from a least-squares non-linear exponential fit is  $797.9 \pm 37.3 \text{ s}$ , where the error corresponds to the 95 % confidence interval. Data points represent average of three different samples. Error bars represent 68% confidence intervals and are smaller than symbol (●). b) The photoluminescence spectrum of the non-irradiated film ( $t = 0 \text{ s}$ , red solid line) displays broad features at  $\sim 475 \text{ nm}$  and  $520 \text{ nm}$ . These are attributed to excimer emission from anthracene dimers. Shoulders around 400 nm, 435 nm and 450 nm correspond to anthracene emission. Upon photodimerization ( $t = 1500 \text{ s}$ , 61% conversion, purple dash dot line), the intensity of the excimer emission diminishes and the photoluminescence spectrum resembles that of isolated anthracene.

Stacked  $\pi$ - $\pi$  anthracene dimers exist in the PIL prior to irradiation with UV, as demonstrated by the blue shift in the 10PIL photoluminescence spectrum upon photocrosslinking (Figure 1b).<sup>62</sup> Specifically, the broad feature near 500 nm (Figure 1b, red solid line) confirms the presence of such  $\pi$ - $\pi$  associations (*i.e.*, excimers).<sup>57</sup> Upon UV irradiation for 1500 s, the excimer band disappears and the resulting emission spectrum is reminiscent of isolated anthracene (Figure 1b, purple dash dot line). This observation indicates that while some anthracene groups in proximity react to form non-emissive dianthracene, others remain unreacted and isolated. Note that although the  $[4\pi + 4\pi]$  cycloaddition is reversible upon exposure to short-wavelength UV radiation (254 nm), both dianthracene and anthracene absorb in this region and eventually reach

a photo-stationary equilibrium with the majority of the anthracene moieties involved in photo-dimerization (Supplementary Information). The presence of  $\pi$ - $\pi$  interactions in the uncrosslinked PIL not only structurally justifies the aforementioned kinetic model that neglects the diffusion limitations in the cycloaddition reaction over the entire range of conversion, but also play a key role in the viscoelastic properties due to formation of labile bonds that serve as dynamic crosslinks (Figure S7a).<sup>44-47</sup> These dynamic crosslinks are not labile at relaxation times shorter than the lifetime of the  $\pi$ - $\pi$  associations, such as those characteristic of segmental and ion motion, and thus influence the local configurational arrangement of polymer chains in a similar manner as chemical crosslinks.

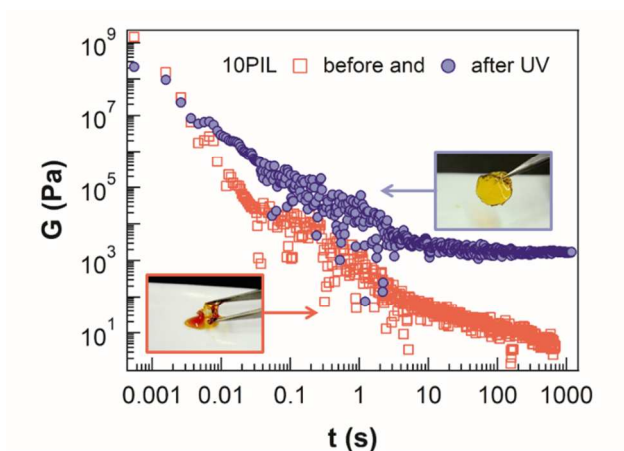


**Figure 2.** Stress relaxation profiles at 50 °C for the 10PIL suggest a change in the terminal mechanical response due to photocrosslinking. 10PIL before ( $\square$ ) and after ( $\bullet$ ) exposure to 365 nm UV radiation for 3 h. The development of a long-time plateau modulus suggests the formation of a lightly crosslinked polymer network. A strain of 1% and 0.1% was respectively applied for the un-crosslinked and crosslinked polymers. The inset images illustrate the change from a viscous liquid to a soft solid.

Photocrosslinking the PIL changes the terminal mechanical response from that of a viscoelastic liquid to that of a soft solid (Figure 2). The stress relaxation profile of 10PIL before exposure to UV is characteristic of a polymer melt with fast relaxation in the shear elastic modulus  $G$  from 5000 kPa to 0.1 kPa in 10 s. After irradiation with UV, the  $\pi$ - $\pi$  stacked anthracene moieties undergo a cycloaddition reaction that chemically crosslinks the polymer resulting in changes in the stress relaxation profile to that of a percolated network above the sol-

gel transition. At long-times there is a plateau modulus of approximately 1.7 kPa which demonstrates that this material is a solid capable of sustaining a mechanical load. The physical appearance (insets in Figure 2) and linear mechanical response (Figure S7) corroborate these observations. Additionally, while the uncrosslinked polymer readily dissolves in organic solvents (e.g., acetonitrile, methanol, DMF, and DMSO) the soft solid that is formed after photocrosslinking is insoluble even after several days. Although the degree of swelling was not systematically investigated, it is qualitatively lower than that characteristic of a polyelectrolyte gel presumably due to the weak electrostatic interactions intrinsic to PILs. More quantitative comparisons between the shear elastic modulus and crosslink concentration are outside the scope of this investigation and only considered in the Supporting Information. It is worth noting that while it is not the objective of this work, the mechanical properties of the crosslinked PIL can be further optimized through an alternative choice for the polymer backbone (*e.g.* PDMS).

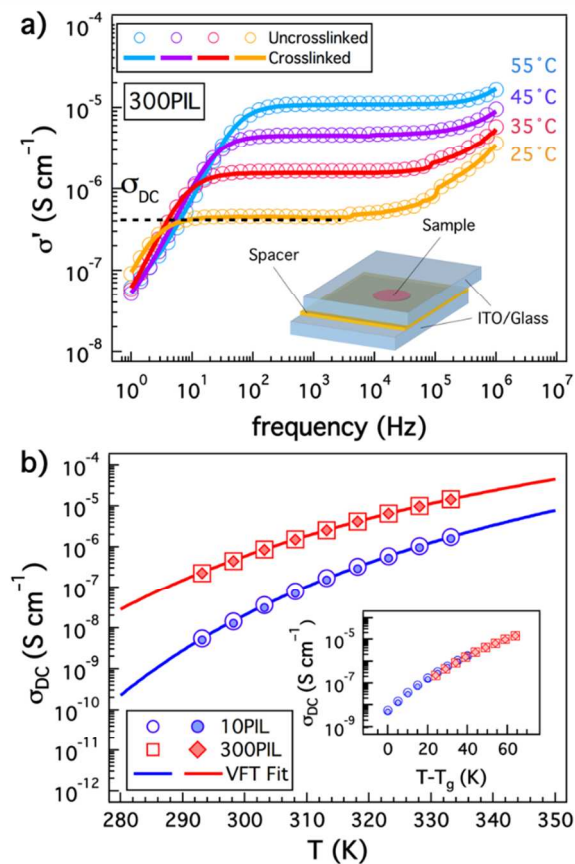


**Figure 3.** Ionic conductivity of anthracene-functionalized PILs before and after crosslinking. a) Real part of complex conductivity as a function of frequency and temperature. The plateau from the frequency independent part of the spectrum was taken as the DC conductivity. The open circles and solid lines respectively correspond to the measurements performed on uncrosslinked and crosslinked (60 min exposure at 298 K) 300PIL. The inset illustrates the schematic of the *in situ* conductivity measurement cell comprising the polymer sandwiched between two ITO/glass transparent electrodes, and separated by a 150  $\mu\text{m}$  Kapton spacer. b) Temperature-dependent ionic conductivity for the PILs. The open and closed symbols are the data for uncrosslinked and crosslinked PILs, respectively, while the solid lines are the VFT fits. The inset illustrates the  $T_g$ -normalized conductivity data for both PILs that fall onto a single master curve. Data points represent the average of three different samples. Error bars represent 68% confidence intervals and are smaller than the symbols.

The enhancement in PIL mechanical properties due to crosslinking does not have deleterious effects on ion transport. To demonstrate this, the ionic conductivity of the PIL was determined using electrochemical impedance spectroscopy, wherein the frequency-independent plateau of the real part of the complex conductivity was attributed to the current resulting from ion conduction (Figure 3a). The specific capacitance of the PIL was also demonstrated to be independent of crosslinking time in the low-frequency regime (Figure S4). It should be noted that the temperature was restricted to 65  $^{\circ}\text{C}$  to mitigate dissociation of the cycloaddition product

dianthracene, which is known to occur to a significant extent at or above 100 °C.<sup>63, 64</sup> A representative Thermo-Gravimetric Analysis (TGA) confirms that neither polymer degradation ( $T_d \approx 270$  °C) nor traces of solvent affect the reported impedance measurements (Figure S6). Figure 3b reveals a perfect overlap at all temperatures between the ionic conductivity of the PIL viscous liquid and that of the soft solid. Interestingly, upon Vogel-Tamman-Fulcher normalization by  $T_g$ , a collapse of the ionic conductivity is evidenced irrespective of molecular weight. These observations demonstrate complete coupling between polymer segmental dynamics and ion transport, as changes in the polymer relaxation times with temperature yield a master curve for the ionic conductivity. The linear dielectric response of this PIL is dictated by mobile ion concentration and mobility, yet these appear to be insensitive to chemical crosslinking. The mobile ion concentration resulting from temperature and solvation do not strongly depend on polymer topology, as ion-ion and ion-monomer interactions are not expected to be significantly affected by chemical crosslinking. However, it is interesting that the formation of a PIL chemical network does not impose restrictions on the internal mobility (*i.e.*,  $T_g$ ).<sup>43</sup> This presumably is a consequence of the  $\pi$ - $\pi$  interactions that influence the polymer segmental dynamics prior to photocrosslinking. In contrast with other PIL networks reported in the literature which exhibit a dramatic reduction in ionic conductivity even at very low crosslink densities due to an increase in  $T_g$ ,<sup>36, 65, 66</sup> the mechanical and ion conducting properties of the photocrosslinkable PIL are decoupled enabling the material to be processed in solution and in the melt, cast into any desired shape, UV-crosslinked, and readily manipulated. The ionic conductivity is acknowledged to be low when compared to similar systems plasticized with ILs or water that accelerate the local segmental dynamics.

The ease of processing that results from the photoconversion of the PIL allows for development of dielectrics amenable to fabrication of thin-film transistors with different geometries but the same material system (*i.e.* substrate, semiconductor, dielectric, and electrodes). This is demonstrated with devices composed of photocrosslinked 300PIL as the dielectric and poly(3-hexylthiophene) (P3HT) as the *p*-type semiconductor in two common geometries (Figure 4a-b). Top-gate and bottom-gate field-effect transistors exhibited reasonably consistent behavior despite differences in device fabrication. The output and transfer characteristics in Figure 4c-f illustrate that both devices exhibit an ON/OFF ratio exceeding 1000 and threshold voltages less than  $|1 \text{ V}|$ . This low-voltage operation, not accessible with conventional gate insulators (*e.g.*,  $\text{SiO}_2$ ), is a consequence of the large sheet charge carrier density that results from the high capacitance ( $1\text{--}10 \mu\text{F}\cdot\text{cm}^{-2}$ ) of the PIL electrical double layer.<sup>9</sup> The relatively slow response time from the ionic moieties tethered to the PIL backbone leads to hysteresis between forward and backward sweeps in the output characteristics, more so in the top-gate geometry due to the larger dielectric thickness. Although this hysteresis can be mitigated by increasing the sweep rate of the device (Figure S9), it is the ionic conductivity of the PIL that ultimately limits performance. As a point of comparison, ion gels exhibit minimal hysteresis in transistor characteristics with sweep rates as large as  $75 \text{ mV}\cdot\text{sec}^{-1}$ , but sacrifice the ability to prevent migration of ion pairs into the semiconductor layer.<sup>67</sup> This observation suggests that a decrease in dielectric thickness or an increase in temperature can improve the switching speed in PIL-gated transistors.

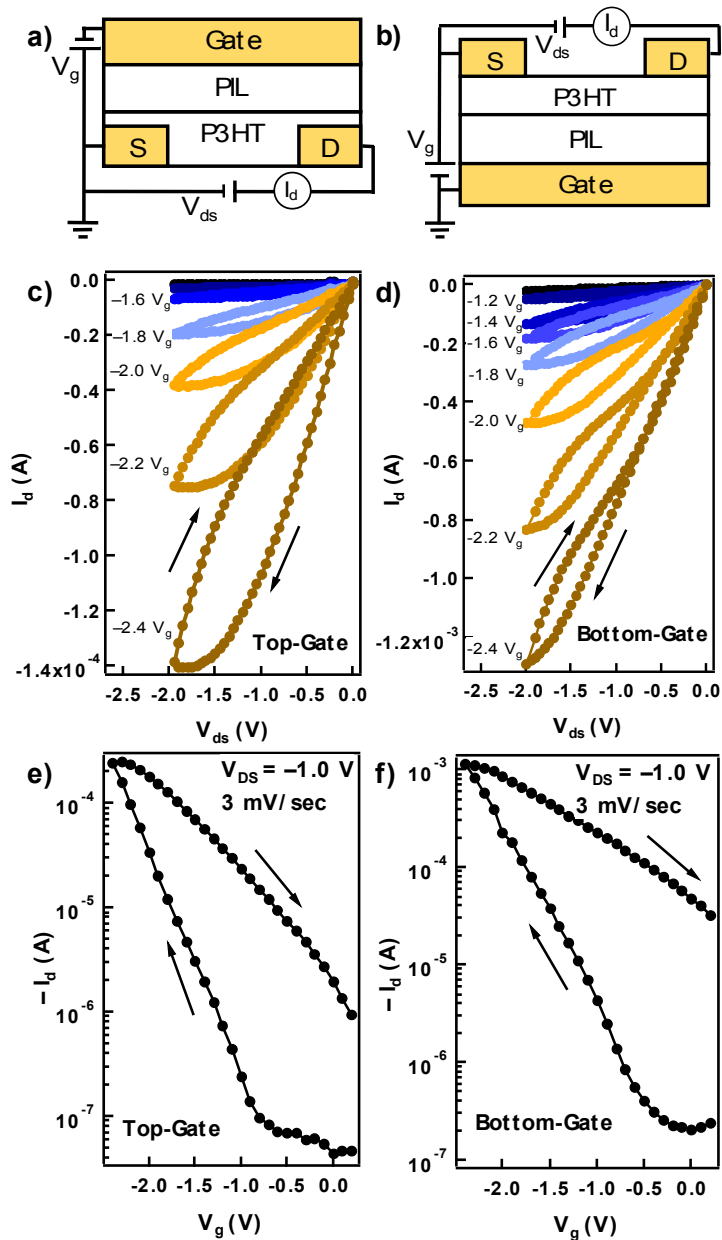


**Figure 4.** Transistor characteristics of two PIL-based organic field-effect transistors. Schematics for the top-gate and bottom-gate structures are shown in (a) and (b), respectively. Sweeping gate voltage from +0.2 to  $-2.4$  V at a sweep rate of  $3.3$  mV  $s^{-1}$  facilitates a turn on voltage less than  $|1$  V and a large ON/OFF ratio as a result of the high capacitance of the PIL. Hysteresis between forward and reverse sweeps is attributed to contributions from the conductivity of the PIL and to the kinetics of infiltration of TFSI into (and out of) P3HT;  $t_{\text{Bottom-Gate}} \sim 5$   $\mu\text{m}$  and  $t_{\text{Top-Gate}} \sim 90$   $\mu\text{m}$ . Output voltage sweeps were completed at  $1000$  mV  $s^{-1}$ .

The UV-activated crosslinking reaction also facilitates patterning of the PIL into sub-mm sized features by use of an appropriate photomask (Supporting Information). This enables lateral control of individual transistors on an integrated circuit, a consideration crucial for the operation

of large-area electronic devices where neighboring transistors may need to be in different ON/OFF states. Here we used a photomask to demonstrate that a 20  $\mu\text{m}$  PIL film can be directly patterned onto a  $\text{SiO}_2$  substrate by crosslinking areas exposed to UV radiation and dissolving the precursor polymer with an orthogonal solvent. The method yields sharp features less than 1 mm in width (Figure 5), though we anticipate that this size can be decreased further by reducing the photomask linewidth. Nonetheless, this simple proof-of-concept illustrates the potential of photocrosslinkable PILs for use in large-area electronics.

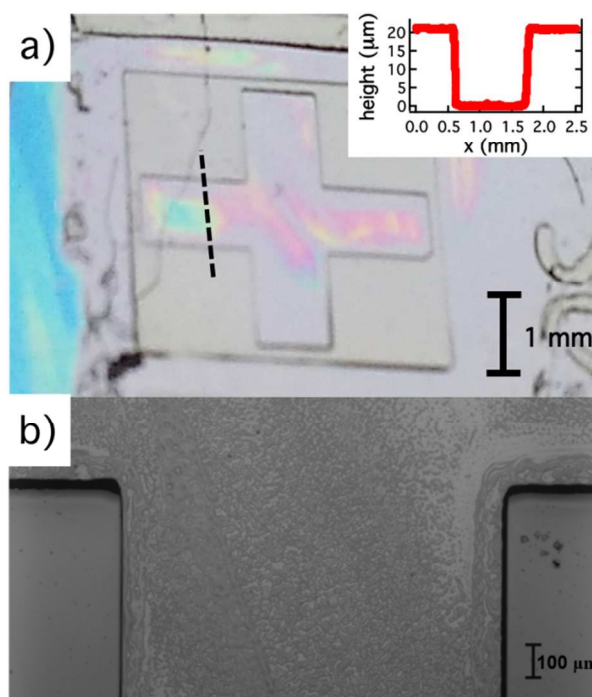


**Figure 5.** The processability and UV-reactivity of the PIL allows for direct patterning as demonstrated with (a) a 20  $\mu\text{m}$  polymer film patterned on a  $\text{Si}/\text{SiO}_2$  substrate. Selectively crosslinking areas of the PIL enables a patterned film with sharp features, illustrated in (inset) the height profile scan, and (b) the optical image.

## Conclusions

Polymeric ionic liquids with tethered anthracene moieties have been photocrosslinked without inducing changes in ionic conductivity. In the melt, these materials are viscous liquids with associating junctions composed of  $\pi$ - $\pi$  stacked anthracene units. Upon exposure to UV, these associations readily become permanent *via*  $[4\pi + 4\pi]$  cycloaddition of anthracene to

produce highly viscoelastic solids based on a lightly crosslinked chemical network. Interestingly, the ionic conductivity of these PILs is decoupled from mechanical properties, as revealed by negligible changes in polymer segmental relaxations and  $T_g$ s after crosslinking. Normalization of the temperature-dependent ionic conductivity by  $T_g$  yields a single master curve for all PIL molecular weights. This molecular design enables the processability required to cast PILs into any desired shape, cure them by UV, and exploit their conducting properties. As proofs of concept, this PIL is incorporated as a dielectric in thin-film transistors with large ON/OFF ratios independent of device fabrication geometry, and directly patterned as films with  $\mu\text{m}$ -size features onto a substrate. Consequently, photocrosslinkable PILs are not only novel functional materials for energy conversion devices, but also serve to address fundamental questions at the interface of polymer science and organic electronics.

### **Supporting Information**

The following files are available free of charge: materials; instrumentation; detailed synthetic procedures; experimental methods for photophysical, mechanical, and dielectric characterization; protocols for transistor fabrication and photopatterning; kinetic modeling of anthracene photodimerization; linear viscoelastic response; frequency-dependent capacitance; discussion on network elasticity; molecular and thermal characterization; sweep-rate dependence of FETs.

### **Corresponding Author**

\*Email: [segalman@ucsb.edu](mailto:segalman@ucsb.edu)

### **Present Addresses**

<sup>§</sup>The Dow Chemical Company, 455 Forest Street, Marlborough, Massachusetts, 01752, United States

<sup>‡</sup>Sciences et Ingénierie de la Matière Molle, CNRS UMR 7615, École Supérieure de Physique et de Chimie Industrielles de la Ville de Paris (ESPCI), ParisTech, PSL Research University, 10 Rue Vauquelin, F-75231, Paris Cedex 05, France.

### **Author Contributions**

B.C.P, E.M.T, N.S.S, S.D.J, and J.M.B acquired the data. B.C.P, G.E.S., E.M.T, N.S.S, S.D.J, and J.M.B analyzed and interpreted the data. M.E.H, M.L.C, and R.A.S critically revised the manuscript. The manuscript was written through contributions of all authors. All authors have given approval to the final version of the manuscript. <sup>†</sup>These authors contributed equally.

### **Notes**

The authors declare no competing financial interest.

### **Acknowledgement**

We gratefully acknowledge the MRSEC Program of the National Science Foundation under Award DMR-1720256 (IRG-2) for the synthesis of the PIL. We also gratefully acknowledge support from the Department of Energy Office of Basic Energy Sciences under Grant No. DE-SC0016390 for all the device and structural characterization. E.M.T. and N.S.S acknowledge the National Science Foundation Graduate Research Fellowship Program Award No. 1650114 for financial support. Any opinions, findings, and conclusions or recommendations expressed in this material are those of the author(s) and do not necessarily reflect the views of the National Science Foundation. N.S.S also gratefully acknowledges the Fannie and John Hertz Foundation and the Holbrook Foundation Fellowship through the UCSB Institute for Energy Efficiency. The authors also thank Costantino Creton and Mehdi Vahdati for helpful discussions.

### **References**

1. N. Nishimura and H. Ohno, *Polymer*, 2014, **55**, 3289-3297.
2. H. Ohno and K. Ito, *Chem. Lett*, 1998, **27**, 751-752.

3. D. Mecerreyes, *Prog. Polym. Sci.*, 2011, **36**, 1629-1648.
4. T. P. Lodge, *Science*, 2008, **321**, 50.
5. T. P. Lodge and T. Ueki, *Acc. Chem. Res.*, 2016, **49**, 2107-2114.
6. R. Hayes, G. G. Warr and R. Atkin, *Chem. Rev.*, 2015, **115**, 6357-6426.
7. H. Ohno, *Electrochim. Acta*, 2001, **46**, 1407-1411.
8. M. Hamed, L. Herlogsson, X. Crispin, R. Marcilla, M. Berggren and O. Inganäs, *Adv. Mater.*, 2009, **21**, 573-577.
9. J.-H. Choi, W. Xie, Y. Gu, C. D. Frisbie and T. P. Lodge, *ACS Appl. Mater. Interfaces*, 2015, **7**, 7294-7302.
10. Q. Thiburce, L. Porcarelli, D. Mecerreyes and A. J. Campbell, *Appl. Phys. Lett.*, 2017, **110**, 233302.
11. E. M. Thomas, B. C. Popere, H. Fang, M. L. Chabinyk and R. A. Segalman, *Chem. Mater.*, 2018, **30**, 2965-2972.
12. M. M. Mahlambi, T. J. Malefetse, B. B. Mamba and R. W. Krause, *J. Polym. Res.*, 2010, **17**, 589-600.
13. J. E. Bara, S. Lessmann, C. J. Gabriel, E. S. Hatakeyama, R. D. Noble and D. L. Gin, *Ind. Eng. Chem. Res.*, 2007, **46**, 5397-5404.
14. Y. Xie, Z. Zhang, T. Jiang, J. He, B. Han, T. Wu and K. Ding, *Angew. Chem. Int. Ed.*, 2007, **46**, 7255-7258.
15. J. Lee, M. J. Panzer, Y. He, T. P. Lodge and C. D. Frisbie, *J. Am. Chem. Soc.*, 2007, **129**, 4532-4533.
16. J. H. Cho, J. Lee, Y. Xia, B. Kim, Y. He, M. J. Renn, T. P. Lodge and C. D. Frisbie, *Nat. Mater.*, 2008, **7**, 900.
17. H. Lee Keun, S. Kang Moon, S. Zhang, Y. Gu, T. P. Lodge and C. D. Frisbie, *Adv. Mater.*, 2012, **24**, 4457-4462.
18. L. Herlogsson, X. Crispin, N. D. Robinson, M. Sandberg, O. J. Hagel, G. Gustafsson and M. Berggren, *Adv. Mater.*, 2007, **19**, 97-101.
19. E. Said, X. Crispin, L. Herlogsson, S. Elhag, N. D. Robinson and M. Berggren, *Appl. Phys. Lett.*, 2006, **89**, 143507.
20. K. H. Lee, S. Zhang, Y. Gu, T. P. Lodge and C. D. Frisbie, *ACS Appl. Mater. Interfaces*, 2013, **5**, 9522-9527.
21. U. H. Choi, Y. Ye, D. Salas de la Cruz, W. Liu, K. I. Winey, Y. A. Elabd, J. Runt and R. H. Colby, *Macromolecules*, 2014, **47**, 777-790.
22. C. M. Evans, C. R. Bridges, G. E. Sanoja, J. Bartels and R. A. Segalman, *ACS Macro Lett.*, 2016, **5**, 925-930.
23. U. H. Choi and R. H. Colby, *Macromolecules*, 2017, **50**, 5582-5591.
24. F. Fan, Y. Wang, T. Hong, M. F. Heres, T. Saito and A. P. Sokolov, *Macromolecules*, 2015, **48**, 4461-4470.
25. S. Liang, M. V. O'Reilly, U. H. Choi, H.-S. Shiao, J. Bartels, Q. Chen, J. Runt, K. I. Winey and R. H. Colby, *Macromolecules*, 2014, **47**, 4428-4437.
26. K. M. Meek and Y. A. Elabd, *J. Mater. Chem. A*, 2015, **3**, 24187-24194.
27. C. M. Bates and F. S. Bates, *Macromolecules*, 2017, **50**, 3-22.
28. L. Gwee, J.-H. Choi, K. I. Winey and Y. A. Elabd, *Polymer*, 2010, **51**, 5516-5524.
29. R. L. Weber, Y. Ye, S. M. Banik, Y. A. Elabd, M. A. Hickner and M. K. Mahanthappa, *J. Polym. Sci. B*, 2011, **49**, 1287-1296.
30. Y. Ye, J.-H. Choi, K. I. Winey and Y. A. Elabd, *Macromolecules*, 2012, **45**, 7027-7035.

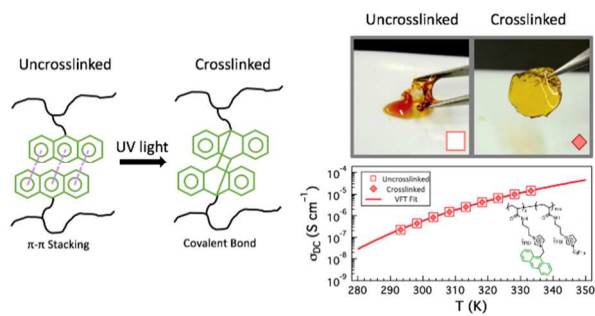
31. J.-H. Choi, Y. Ye, Y. A. Elabd and K. I. Winey, *Macromolecules*, 2013, **46**, 5290-5300.
32. G. Sudre, S. Inceoglu, P. Cotanda and N. P. Balsara, *Macromolecules*, 2013, **46**, 1519-1527.
33. P. Cotanda, G. Sudre, M. A. Modestino, X. C. Chen and N. P. Balsara, *Macromolecules*, 2014, **47**, 7540-7547.
34. C. M. Evans, G. E. Sanoja, B. C. Popere and R. A. Segalman, *Macromolecules*, 2016, **49**, 395-404.
35. G. E. Sanoja, B. C. Popere, B. S. Beckingham, C. M. Evans, N. A. Lynd and R. A. Segalman, *Macromolecules*, 2016, **49**, 2216-2223.
36. S. Washiro, M. Yoshizawa, H. Nakajima and H. Ohno, *Polymer*, 2004, **45**, 1577-1582.
37. P.-G. de Gennes, *Scaling Concepts in Polymer Physics*, Cornell University Press, Ithaca and London, 1979.
38. R. J. Wojtecki, M. A. Meador and S. J. Rowan, *Nat. Mater*, 2010, **10**, 14.
39. L. A. Connal, R. Vestberg, C. J. Hawker and G. G. Qiao, *Adv. Funct. Mater*, 2008, **18**, 3315-3322.
40. T. F. Miller, Z.-G. Wang, G. W. Coates and N. P. Balsara, *Acc. Chem. Res*, 2017, **50**, 590-593.
41. J. Newman and K. E. Thomas-Alyea, *Electrochemical Systems*, John Wiley & Sons, Inc., Hoboken, NJ, 3rd edn., 2004.
42. W. M. Deen, *Analysis of Transport Phenomena*, Oxford University Press, 2nd edn., 2012.
43. T. G. Fox and S. Loshaek, *J. Polym. Sci. A*, 1955, **15**, 371-390.
44. M. S. Green and A. V. Tobolsky, *J. Chem. Phys*, 1946, **14**, 80-92.
45. F. Tanaka and S. F. Edwards, *Macromolecules*, 1992, **25**, 1516-1523.
46. L. Leibler, M. Rubinstein and R. H. Colby, *Macromolecules*, 1991, **24**, 4701-4707.
47. M. Rubinstein and A. N. Semenov, *Macromolecules*, 2001, **34**, 1058-1068.
48. R. Hoffmann and R. B. Woodward, *Acc. Chem. Res*, 1968, **1**, 17-22.
49. M. O'Donnell, *Nature*, 1968, **218**, 460-461.
50. M. D. Green, D. Salas-de la Cruz, Y. Ye, J. M. Layman, Y. A. Elabd, K. I. Winey and T. E. Long, *Macromol. Chem. Phys*, 2011, **212**, 2522-2528.
51. H. He, M. Zhong, B. Adzima, D. Luebke, H. Nulwala and K. Matyjaszewski, *J. Am. Chem. Soc*, 2013, **135**, 4227-4230.
52. R. Murali and A. Eisenberg, in *Structure and Properties of Ionomers*, eds. M. Pineri and A. Eisenberg, Springer Netherlands, Dordrecht, 1987, DOI: 10.1007/978-94-009-3829-8\_25, pp. 307-319.
53. S. Lascaud, M. Perrier, A. Vallee, S. Besner, J. Prud'homme and M. Armand, *Macromolecules*, 1994, **27**, 7469-7477.
54. M. A. B. H. Susan, T. Kaneko, A. Noda and M. Watanabe, *J. Am. Chem. Soc*, 2005, **127**, 4976-4983.
55. R. N. Jones, *Chem. Rev*, 1947, **41**, 353-371.
56. E. A. Chandross, J. Ferguson and E. G. McRae, *J. Chem. Phys*, 1966, **45**, 3546-3553.
57. J. S. Hargreaves and S. E. Webber, *Macromolecules*, 1984, **17**, 235-240.
58. J. S. Hargreaves, *J. Polym. Sci. A*, 1989, **27**, 203-216.
59. J.-F. Xu, Y.-Z. Chen, L.-Z. Wu, C.-H. Tung and Q.-Z. Yang, *Org. Lett*, 2013, **15**, 6148-6151.
60. G. W. Breton and X. Vang, *J. Chem. Ed.*, 1998, **75**, 81.

61. H. Bouas-Laurent, A. Castellan, J.-P. Desvergne and R. Lapouyade, *Chem. Soc. Rev.*, 2001, **30**, 248-263.
62. G. F. Moore, *Nature*, 1966, **212**, 1452-1453.
63. S. Grimme, S. D. Peyerimhoff, H. Bouas-Laurent, J.-P. Desvergne, H.-D. Becker, S. M. Sarge and H. Dreeskamp, *Phys. Chem. Chem. Phys.*, 1999, **1**, 2457-2462.
64. M. Yokoe, K. Yamauchi and T. E. Long, *J. Polym. Sci. A*, 2016, **54**, 2302-2311.
65. B. Altava, V. Compañ, A. Andrio, L. F. del Castillo, S. Mollá, M. I. Burguete, E. García-Verdugo and S. V. Luis, *Polymer*, 2015, **72**, 69-81.
66. T. C. Rhoades, J. C. Wistrom, J. R. Daniel and K. M. Miller, *Polymer*, 2016, **100**, 1-9.
67. J. Lee, L. G. Kaake, J. H. Cho, X. Y. Zhu, T. P. Lodge and C. D. Frisbie, *J. Phys. Chem. C*, 2009, **113**, 8972-8981.

## For Table of Contents Use Only

### Photocrosslinking Polymeric Ionic Liquids *via* Anthracene Cycloaddition for Organic Electronics

*Bhooshan C. Popere, Gabriel E. Sanoja, Elayne M. Thomas, Nicole S. Schausser, Seamus D. Jones, Joshua M. Bartels, Matthew E. Helgeson, Michael C. Chabinyc, and Rachel E. Segalman*



Uncrosslinked

Crosslinked

Uncrosslinked

Crosslinked

